# Simulation models of Dengue transmission in Funchal, Madeira Island: influence of seasonality

Donald Salami[1*], César Capinha[2], Carla Alexandra Sousa[3], Maria do Rosário Oliveira Martins[3], Cynthia Lord[4]

[1] Global Public Health Doctoral Programme, Instituto de Higiene e Medicina Tropical, Universidade Nova de Lisboa, Lisbon, Portugal

[2] Centro de Estudos Geográficos, Instituto de Geografia e Ordenamento do Território, Universidade de Lisboa, Lisbon, Portugal

[3] Global Health and Tropical Medicine, Instituto de Higiene e Medicina Tropical, Universidade Nova de Lisboa, Lisbon, Portugal

[4] Florida Medical Entomology Laboratory, Institute of Food and Agricultural Sciences, University of Florida, Vero Beach, Florida, United States.

* Corresponding author

Email: donald.salami@gmail.com (DS)

## Abstract

The recent emergence and established presence of *Aedes aegypti* in the Autonomous region of Madeira, Portugal, was responsible for the first autochthonous outbreak of dengue in Europe. The island has not reported any dengue cases since the outbreak in 2012. However, there is a high risk that an introduction of the virus would result in another autochthonous outbreak given the presence of the vector and permissive environmental conditions. Understanding the dynamics of a potential epidemic is critical for targeted local control strategies.

Here, we adapt a deterministic model for the transmission of dengue in *A. aegypti* mosquitoes. The model integrates empirical and mechanistic parameters for virus transmission, under seasonally varying temperatures for Funchal, Madeira Island. We examine the epidemic dynamics as triggered by the arrival date of an infectious individual; the influence of seasonal temperature mean and variation on the epidemic dynamics; and performed a sensitivity analysis on the following quantities of interest: the epidemic peak size, time to peak and the final epidemic size.

Our results demonstrate the potential for year-round transmission of dengue, with the arrival date significantly affecting the distribution of the timing and peak size of the epidemic. Late summer to early autumn arrivals is more likely to produce larger epidemics within a short peak time. Epidemics within this favorable period had an average of 22% of the susceptible population infected at the peak, at an average peak time of 82 days. We also demonstrated that seasonal temperature variation dramatically affects the epidemic dynamics, with warmer starting temperatures producing peaks more quickly after introduction and larger epidemics. Overall our quantities of interest were most sensitive to variance in date of arrival, seasonal temperature, biting rate, transmission rates, and the mosquito population; the magnitude of sensitivity differs across quantities.

Our model could serve as a useful guide in the development of effective local control and mitigation strategies for dengue fever in Madeira Island.

## Introduction

Dengue is notably the most important mosquito-borne viral disease, with approximately half the world's population at risk of infection [1]. This arboviral disease, caused by a virus of the Flaviviridae family, has gained renewed global attention due to its wide geographical spread and increased burden in recent years. The spread of the disease is in concordance with the geographical expansion of its primary vector (i.e. *Aedes aegypti*), characterized by the presence of a suitable climate and increase in global trade and travel [2, 3].

A paradigmatic example of the recent spread of dengue and of its epidemic potential was demonstrated in Madeira Island, an autonomous region of Portugal. *A. aegypti* was first detected in Funchal, the capital city of Madeira Island, in 2005 and by October 2012 the island reported its first autochthonous case of Dengue serotype 1 (DENV 1) [4]. The importance of this epidemic is demonstrated by three main reasons: (1) It was the first sustained autochthonous transmission of dengue in the European Union since the 1920s [5]; (2) its size, with 1080 confirmed cases (of the 2168 probable cases reported) and 78 cases reported in 13 other European countries in travelers returning from Madeira [6]; and (3) the rapid time course of the epidemic, that peaked within a month after the official report of the first case in October [7].

To understand the complexities of this outbreak, Lourenco and Recker [8] developed an ento-epidemiological mathematical model to explore the ecological conditions and transmission dynamics. Their findings suggest the virus was introduced over a month before cases were reported (in August). In their model, asymptomatic circulation occurred before the two initial autochthonous cases were reported in October, maintaining the virus in the population. Furthermore, their findings indicate that the transmission dynamics and eventual epidemic burnout was driven predominantly by the influence of temperature on the life history traits of the mosquitoes (incubation period, mosquito mortality and aquatic developmental rates). The seasonal drop in autumn temperatures led to a reduction of the vectorial capacity and effectively stopped the virus propagation.

Their findings are consistent with previous experimental work addressing the strong influence of temperature on the life history traits of the mosquitoes and arbovirus transmissions

[9-12]. Likewise, many existing mechanistic transmission models have integrated the effects of temperature on mosquito traits to understand how it influences the probability and magnitude of dengue transmissions [13-17]. Other recent work examined the influence of seasonal variation in temperature on the epidemic magnitude and duration [18, 19]. These models emphasize the strong, nonlinear (often unimodal) influence of temperature and seasonality on dengue transmission and epidemic dynamics.

Expanding on previous work, we here explore the impact of seasonal temperature variations on the potential epidemic dynamics on Madeira Island. It is imperative to explore the influence of seasonality, as Madeira Island presents with a range of contrasting bioclimates as a result of its heterogeneous landscape and strong influence from the Gulf Stream and Canary current [20]. The southern coastal regions of the island (including Funchal), at low altitudes, have higher annual temperatures in comparison to the northern coastal regions or inland regions with higher altitudes [20, 21]. In addition, though the island has not reported any dengue cases since the outbreak in 2012, it is likely that new introductions would result in local transmission given the presence of the vector and permissive environmental conditions. A recent vector competence study with *A. aegypti* from Madeira reported virus transmission potential (virus in saliva) from 2 Madeira populations, although the proportions transmitting were low (transmission rate of 18%, 14 days post-infection) [22]. This demonstrates the potential risk for the local transmission of dengue 2 serotype (DENV 2) if introduced on the island. With an increase in co-circulation of all dengue serotypes (DENV 1-4) worldwide [23, 24], and Madeira's increasing lure as a popular year-round travel destination, a potential introduction is likely [25].

We incorporate a standard deterministic SEI-SEIR transmission model parameterized from existing literature and available field data. The main goals of this model are: (1) to examine the epidemic dynamics in Funchal, Madeira as triggered by the arrival of an infectious individual at different timepoints during the year; and (2) to examine the influence of seasonal temperature mean and variation on epidemic dynamics. To do this, we employed a different modeling framework from that of [8], in that our model explicitly accounts for seasonality and temperature dependence in the transmission dynamics. Likewise, we explore epidemiologically relevant

outcomes of epidemic size, peak incidence and time to peak, rather than basic reproduction number or vectorial capacity, which are more complex measures of epidemic dynamics.

## Methods

### Model framework

We adapt a deterministic compartmental vector-host transmission model exploring chikungunya virus invasion in Florida, USA with *A. aegypti* and *Aedes albopictus* mosquitoes, from Lord et al. (unpublished work). This was adapted into a standard SEI-SEIR transmission model with one vector, similar to others used in modelling dengue transmission (e.g. in [26-29]).

The SEI component of our model describes the vector population, represented as susceptible ($S_v$), exposed ($E_v$), and infectious ($I_v$). Our models explicitly consider a single vector and a single life stage, i.e. adult females of *A. aegypti*. Mosquitoes enter the susceptible class through a recruitment term, based on observed seasonality patterns from field data in Funchal [30]. The recruitment term does not explicitly model the aquatic (eggs, larvae, and pupae) stage of mosquitoes and is not linked to current population size, but explicitly includes seasonality in recruitment to the adult female population. A susceptible mosquito moves into the exposed class ($E_v$), after biting an infectious human and becoming infected with dengue virus. After a temperature dependent extrinsic incubation period, surviving mosquitoes get transferred to the infectious class ($I_v$). They remain in the infectious class until death, due to the assumption of the absence of immune response. Mosquitoes leave the system through a temperature dependent mortality function. We assume the virus infection does not affect the lifespan of the mosquitoes and that there is no significant vertical transmission.

The SEIR component of our model describes the human population represented as susceptible ($S_h$), exposed (infected but not infectious) ($E_h$), infectious ($I_h$), and recovered (immune) ($R_h$). Our model assumes the human population ($N_h$) to be constant, not subject to demography as we considered a single outbreak with a duration in the order of a year. A susceptible individual enters the exposed class ($E_h$) after being successfully infected, by an infectious mosquito bite. We do not explicitly account for repeated biting, interrupted feeds or

alternative host preferences. We also assume that not every infectious bite leads to successful human infection. Once a human individual is exposed, they enter an intrinsic incubation period, until they become infectious. They then move to the infectious class ($I_h$) and can transmit the virus back to a susceptible mosquito. We assume that humans stay infectious for a period after which they recover. Once a human individual enters the recovered/immune class ($R_h$), we assume a lifelong immunity, as multiple co-circulating serotypes of dengue virus are not considered. A resulting schematic representation of the model is shown in Fig 1.

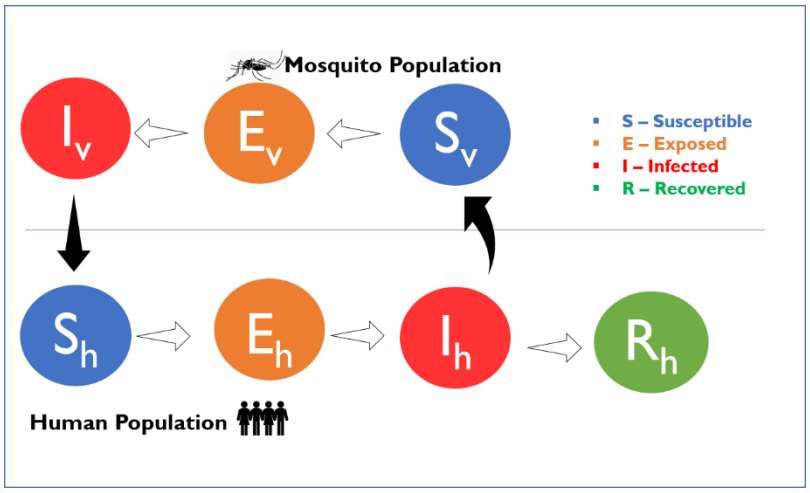


**Fig 1. Schematic representation of the model.** $S_v$, $E_v$, and $I_v$ represent the susceptible, exposed, and infectious compartments of the mosquito population. $S_h$, $E_h$, $I_h$, and $R_h$ represent the susceptible, exposed, infectious, and recovered compartments of the human population, respectively. The outline arrows are the transition from one compartment to the next, and the black filled arrows are the direction of transmission.

## Model equations

Our model is defined by the following ordinary differential equations:

$$\frac{dS_v}{dt} = \rho - \frac{a\,\beta_{h\to v}}{N_h} I_h S_v - \mu_v S_v \qquad (1)$$

$$\frac{dE_v}{dt} = \frac{a\,\beta_{h\to v}}{N_h} I_h S_v - \gamma_v E_v - \mu_v E_v \qquad (2)$$

$$\frac{dI_v}{dt} = \gamma_v E_v - \mu_v I_v \qquad (3)$$

$$N_v = S_v + E_v + I_v \quad (4)$$

$$\frac{dS_h}{dt} = -\frac{a\,\beta_{v\to h}}{N_h} S_h I_v \quad (5)$$

$$\frac{dE_h}{dt} = \frac{a\,\beta_{v\to h}}{N_h} S_h I_v - \gamma_h E_h \quad (6)$$

$$\frac{dI_h}{dt} = \gamma_h E_h - \eta_h I_h \quad (7)$$

$$\frac{dR_h}{dt} = \eta_h I_h \quad (8)$$

$$N_h = S_h + E_h + I_h + R_h \quad (9)$$

Here, the coefficient $\rho$ is the mosquito recruitment term (expanded below); $a$ is the biting rate; $\beta_{h\to v}$ and $\beta_{v\to h}$ are the human-to-mosquito and mosquito-to-human transmission rates, respectively; $1/\gamma_h$ and $1/\eta_h$ represent the intrinsic incubation and human infectivity periods; $1/\gamma_v$ and $\mu_v$ represent the extrinsic incubation period and mortality rate for mosquitoes (temperature dependent, details below). The state variables and parameters used for our model are displayed in Tables 1 and 2, respectively.

**Table 1. State variables for the model.**

| Variables | Description |
|---|---|
| $S_v$ | Number of susceptible mosquitoes |
| $E_v$ | Number of exposed mosquitoes |
| $I_v$ | Number of infectious mosquitoes |
| $N_v$ | Total mosquito population size |
| $S_h$ | Number of susceptible humans |
| $E_h$ | Number of exposed humans |
| $I_h$ | Number of infectious humans |
| $R_h$ | Number of recovered humans |
| $N_h$ | Total human population size |

**Table 2. Definitions and ranges of the model's parameters.**

| Parameter | Description | Default Value | Range | Reference |
|---|---|---|---|---|
| $r_\delta$ | Number of mosquitoes per host in the unimodal peak phase | 2 | 2 – 6 | [8, 31, 32] |
| $p_{base}$ | Proportion of mosquitoes in baseline recruitment | 0.05 | | [8, 33] |
| $iv$ | The interval between baseline pulses (days)[1] | 5 | 2 – 7 | [33] |
| $q$ | Timing of unimodal peak (days)[1] | 266 | 255 –276 | [33] |
| $\sigma$ | The variance of the unimodal peak (days)[1] | 29 | | [33] |
| $R_{tot}$ | Total mosquito recruitment (population size)[2] | | | Calculated based on default value and range for $r_\delta$ above. Used in the sensitivity analysis. |
| $a$ | Mosquito biting rate | 0.4 | 0.33 – 1.0 | [34, 35] |
| $\beta_{h\to v}$ | Rate of transmission from human to mosquito | 0.33 | 0.1 – 0.75 | [27, 31, 36] |
| $\beta_{v\to h}$ | Rate of transmission from mosquito to human | 0.33 | 0.1 – 0.75 | [27, 31, 36] |
| $\mu_v$ | Mortality rate of mosquitoes under optimal temperatures [3] | 0.04 | 0.02 – 0.06 | [13, 17] |
| $\mu_{vs}$ | The slope of mortality function | 0.05 | | [13, 37] |
| $\gamma_v$ | Virus extrinsic incubation rate (at 22.5°C) | 0.04 | 0.04 – 0.07 | [17, 38] |
| $\gamma_{vs}$ | Slope of extrinsic incubation function | 0.008 | | [38] |
| $1/\gamma_h$ | Intrinsic incubation period (days) | 6 | | [39, 40] |
| $1/\eta_h$ | Human infectious period (days) | 5 | | [8, 35, 41, 42] |
| $N_h$ | The population size of humans (constant) | 30000 | | [43] |
| $t_{crit}$ | Date of arrival of infectious human (days) | 181 | 1 – 365 | |
| $T_{mean}$ | Mean annual temperature (°C) | 20 | 19 - 21 | [44] |
| $T_{range}$ | Temperature range (°C)[4] | 5 | 4 - 6 | [44] |

[1] Default value and range are estimates to reflect the observed seasonal activity, not an explicit fit to the island's entomological data; [2] See equation 15, also note this parameter was used in the sensitivity analysis to allow

estimation of the relative importance of the total recruitment; [3] Mosquitoes optimal survival range: ($15 > T < 30$°C); [4] Temperature range is given by($T_{max} - T_{min}$).

**Mosquito recruitment**. The coefficient ($\rho$) in equation (1) above is the daily recruitment term of susceptible mosquitoes. The total number of female mosquitoes recruited into the population over the year is divided into two main phases: baseline, year-round recruitment, and a unimodal peak season recruitment. This is based on the seasonal pattern of mosquitoes on the island observed from the *A. aegypti* mosquito entomological surveillance by the Institute of health administration, IP-RAM and the Funchal natural history museum [30, 45]. Weekly mosquito trap data is geo-processed and spatial analyzed to identify areas with mosquito activity based on the presence/absence of eggs, the number of eggs and adult mosquitoes captured [30].

Visual inspection of the entomological data for the years 2012 – 2019 (weekly time-series graphs of the cumulative number of eggs and adult mosquitoes) [33] demonstrate a unimodal seasonal pattern for mosquito activity during the entomological season. The unimodal peak starts around June through to early December, with other months of the year (i.e. January to May) having little to no activity. Using a Gaussian curve, we estimated the timeline for our unimodal peak recruitment to reflect this seasonal pattern as best possible.

Actual quantifications of mosquito population density remain a grey area. However, the majority of dengue models [8, 27, 31, 32, 46] have adopted the use of a mosquito-to-human ratio of 2:1. We adopted this framework for setting the estimated number of mosquitoes recruited during the unimodal peak season ($r_\delta$). From the derived number of mosquitoes recruited during the peak season, we assumed an additional 5% to be added in the baseline, year-round recruitment ($p_{base}$). The recruitment of susceptible mosquitoes is specified by the following equations:

$$\rho(t) = \rho_b\ (t) + R_{peak}\delta(t) \qquad (10)$$

Where,

$$\delta\,(t) = \frac{1}{2\pi\sigma_k}\ exp\left(\frac{1(q_k - t)^2}{2\sigma_k^2}\right) \qquad (11)$$

$$\rho_b(t) = \frac{R_{base}}{iv} \quad (12)$$

$$R_{peak} = r_\delta N_h \quad (13)$$

$$R_{base} = R_{peak} p_{base} \quad (14)$$

$$R_{tot} = R_{peak} + R_{base} \quad (15)$$

Here, $\rho(t)$ represents the number of adult female mosquitoes recruited per time step; $\delta\,(t)$ is a Gaussian distribution for the number of mosquitoes added to the population daily, during the unimodal peak season; $\rho_b(t)$ is the number of mosquitoes added to the population at intervals ($iv$) during the all-year round recruitment. $R_{peak}$ is the total number of mosquitoes recruited during the unimodal peak season; $R_{base}$ is the total number of mosquitoes recruited during the baseline, year-round recruitment; $R_{tot}$ is the total number of mosquitoes recruited into the population over the year.

**Seasonal forcing.** To introduce seasonality in our model, we allowed temperature to vary over time by sinusoidally forcing [47]. The daily mean temperature was modelled as a cosine curve with a period of 365 days as specified below:

$$T\,(t) = \frac{T_{max} - T_{min}}{2} * \left(-\cos\left(\frac{2\pi(t-\omega)}{365}\right)\right) + T_{mean} \quad (16)$$

Here, $T_{max}$, $T_{mean}$, and $T_{max}$ are the average daily maximum, mean, and minimum temperatures over the year, ($t$) is time measured in days and ($\omega$) is the phase shift to align the cosine function with the seasonal factors in Funchal. For our temperature model calibration, we extracted a 10 year (2008 – 2018) historical daily temperature data for Funchal from Weather Underground [44]. Utilizing the mean of the minimum, average and maximum daily mean temperatures, we set estimates for our seasonality parameters. The mode minimum temperature across the years occurred on February 15; hence we set our phase shift at this point to reflect the long-term average conditions in Funchal, Madeira ($T_{max}$= 22° C, $T_{mean}$= 20°C, $T_{min}$= 17°C).

**Temperature dependent parameters.** The extrinsic incubation period ($\gamma_v$) is modelled to be temperature dependent, modified from [48]. Using a linear temperature function, specified by a slope ($\gamma_{vs}$), the rate near the midpoint of the plausible temperatures range for vectorial capacity (set at 22.5°C), and a defined lower temperature threshold (set at 10ºC, at which point ($\gamma_v$) equals zero). Mortality rates ($\mu_v$) for mosquitoes was modelled as a function of temperature using a mechanistic thermal response curve as described in [13]. They fitted their data as a complex polynomial resulting in a basin- shape curve, with optimal temperature for mosquito's survival set at a range of $15℃ > T < 30℃$. Based on a preliminary exploration of changes to the mortality function, we modified the fitted polynomial to a piecewise linear curve with fixed, minimal mortality in the same temperature range. Mortality rate then increases quickly and linearly at temperatures outside this lower and upper bound, as specified by the function slope ($\mu_{vs}$).

**Starting conditions**

The model requires an estimate of each state variable (humans and mosquitoes in each class), along with estimates or values chosen from distributions for each parameter. Our parameter values are based on multiple citations from reviewed literature of previous empirical studies or lab trials and expert opinion. We emphasize previous studies within the context of Funchal, Madeira Island (since our main objective was to parameterize the model for the island) and chose parameter ranges to reflect conditions in Funchal.

The model assumes a homogeneously mixed population, with a total human population set at a constant 30,000 (representative of the population of the most populous civil parish – *Santo António* – in the municipality of Funchal and the island) [43]. Since the human components of the transmission cycle are not seasonal, we set the intrinsic incubation ($1/\gamma_h$) and the infectious period ($1/\eta_h$) to constants of 6 and 5 days respectively. For this model, we considered only a single dengue serotype. Based on our mosquito recruitment term, the initial susceptible mosquito population is set as the number of females ($\rho_b(t)$) added to the population at intervals ($iv$), as calculated in equation (12) above. With all infectious classes for both human

and mosquitoes set to zero, an infection is triggered by the arrival of one infectious human on a specified day ($t_{crit}$) into the fully susceptible population. The default initial conditions are thus: $(S_h;\ E_h;\ I_h;\ R_h;\ S_v;\ E_v;\ I_v) = (N_h;\ 0;\ 0;\ 0;\ p_b(t);\ 0;\ 0)$ where $N_h = 30{,}000$.

Simulations were set to start at the coldest day in the annual cycle (i.e. February 15) and ran for 730 days thereafter (allowing for simulation with $t_{crit}$ later in the year). We set an arbitrary cut-off value for the infectious human, exposed and infectious mosquitoes classes: if ($I_h$ , $E_v$ , $I_v$, all $<0.5$) the simulation is terminated and restarted with the classes set to zero. This cutoff is necessary otherwise extremely low levels of infection may persist for long periods; in the natural system, there would be a high probability that the virus would go extinct [49].

We performed a preliminary exploration of parameter values to determine their effects on transmission. The choice of the final parameter values was based on permissibility for transmission. The preliminary exploration also informed the initial conditions (described above) and parameter ranges for sensitivity analyses (Table 2).

Model simulations were performed using the governing systems of differential equations of MATLAB's inbuilt routine "ode45" [50]. Simulation outputs were processed in the R Programming Language version 3.5.3 [51].

**Quantities of interest**

Given that a simulation evolves into an epidemic (defined as ($I_h > 2$), after the virus introduction), we analyze each simulation for the following quantities of interest (QOI): the epidemic peak size (maximum human infected ($maxI_h$) at any given point during the simulation); time to peak infection in humans (time from introduction to $maxI_h$, as $tmaxI_h$); the final epidemic size, which represents a measure of epidemic suitability (cumulative proportion of humans infected, $cumI_h/N_h$, at the final time step).

**Initial introduction and epidemic dynamics**

Firstly, we examine the variability in epidemic dynamics, as a result of different arrival dates of an infectious human in a susceptible population. To do this, we ran simulations for all 365 calendar days of the year ($t_{crit}$ = 1, 2, 3…365), with all other parameters fixed at their default values and initial conditions (Table 2). Each simulation was started on February 15 (the phase shift in the annual cycle) and ran for 2 years.

**Seasonal variance and epidemic dynamics**

Next, we examine the epidemic dynamics as a function of seasonal temperature variation. Utilizing the same compartmental framework with default initial conditions and parameter values, we ran sets of simulations under two different temperature regimes [18]. First, we simulated a set of temperature regimes as observed in the historical decadal data for Funchal, Madeira. The mean temperature varied from 19.0 ºC to 21.0 ºC in increments of 0.2 ºC, while the temperature range (i.e. $T_{max} - T_{min}$) varied from 4.0 ºC to 6.0 ºC, in the same increments of 0.2 ºC, resulting in 121 simulation runs. The variability in epidemic dynamics is then examined as a function of starting temperature. Starting temperature is defined as the temperature on the day of introduction of the virus ($t_{crit}$), as derived from the temperature curves.

Next, we simulate a wider set of temperature regimes to examine plausible future forcing scenarios based on near-term projections of seasonal temperature changes in the region of Madeira Island [52]. Mean temperature was varied between 15.0 ºC to 30.0 ºC in increments of 0.2 ºC, while range varied from 0.0 ºC to 15.0 ºC in increments of 0.2 ºC (i.e. a total of 5776 simulation runs). It is worth noting that most of the temperatures in this regime are outside projected changes for the island's region, and very unlikely to occur in Funchal. However, by simulating a wider set of temperature regimes, we are able to characterize uncertainties and probable outcomes of a local epidemic across other regions on the island. This also allows us to simulate similar extreme temperature conditions already recorded on the Funchal in recent times (for example, high temperatures of 37.8ºC on August 5, 2016, and 26.5 ºC on December 5, 2018 [53, 54].

**Model sensitivity analysis**

To characterize the model parameters exerting the most influence on our quantities of interest, we performed a variance-based global sensitivity analysis, using a combination of Latin hypercube sampling (LHS) and a multi-model inference on regression-based models. LHS is a stratified Monte Carlo sampling technique, where specified parameter distributions are divided into (*M)* equiprobable intervals, and then sampled, here (*M*) is the sample size. The entire range of each parameter is explored, by sampling each interval for each parameter only once without replacement. Parameters values are then randomly resorted into sets to use for simulation. The LHS method assumes that the sampling is performed independently for each parameter, thereby allowing for an un-biased estimate [55, 56]. Parameter ranges for sampling were derived from existing literature, expert opinion and field-based data (Table 2), we assumed a uniform distribution for all parameter values. LHS sampling was programmed in MATLAB.

Multi-model inference on a generalized least square (GLS) regression was used to estimate the relative importance of the input parameters. Multi-model inference uses the information-theoretic approach to offer a more objective way to assess the relative importance of input variables by inferring all possible models from a defined candidate set [57, 58]. A vector of the input parameters ($x_p$) were fitted into all possible unique models and then ranked from best to worst, based on Akaike information criterion (AIC) values. An estimate of the relative importance of a single parameter ($p$) was then calculated by summing the Akaike weights ($w$) across all fitted models where parameter ($p$) occurs. Akaike weights are normalized, such that the sum over all models considered is 1. The relative importance of parameter ($p$) was quantified by the sum ($w$) for the parameter. The larger the sum of the weight (between 0 and 1 by definition) the more important the parameter is, relative to the other parameters [58]. Input parameters were then ranked in terms of their importance to the quantities of interest. Multi-model inference analysis was done using the *glmulti* R package [59].

Our analysis considered two separate candidate model sets, one with main effects only and one with main effects and pairwise (first order) interactions of input parameters on our

quantities of interest. The first analysis (i.e. main effects only) utilized all possible unique candidate models through an exhaustive screening method. However, the second analysis utilized only a subset of all possible candidate models, using a genetic algorithm [59], as it was infeasible to consider all. Our confidence set (for both analysis) was defined as all models within two Akaike information criterion (AIC) unit difference (ΔAIC) from the best model (see appendix for more details). Models in the confidence set are averaged to produce the relative importance and coefficient estimates of input parameters. Note, before the multi-model inference fitting, we normalized the input parameters (by centering on zero and scale to unit variance) to allow comparison of resulting model-averaged estimates on a common scale.

## Results

### Initial introduction and epidemic dynamics

We examined the timing and size of the epidemic peak as a function of different arrival dates of an infectious human into the susceptible population. An epidemic outbreak occurred for all simulated arrival dates in the year, with varying epidemic peak size and time to peak, indicating that the default parameter values used for simulations were permissive for transmission. Most simulations responded unimodally with peaks occurring few weeks after the arrival of an infectious human, this was typical for summer (June – August) arrivals (Figs 2A and 2B). However, some simulations responded bimodally, i.e. an initial small outbreak, then a prolonged low-level transmission until another outbreak occurs (Figs 2C and 2D). This prolonged transmission was typical for arrival dates at the start of the winter (i.e. arrival dates of the 12 to 19 December).

We examine this behavior further by comparing the disease progression in the human population with that of the mosquito population (Fig 2D). Simulations with a late arrival of the infectious human in December had a lower chance to evolve into a large unimodal outbreak, because of the depletion of the mosquito population. Following the initial outbreak, a low transmission is maintained until the next seasonal peak recruitment of the mosquitoes, before another outbreak. This means the dynamics of the epidemic, is also modulated by the temporal dynamics of the mosquito population, however, this is not the focus of our analysis.

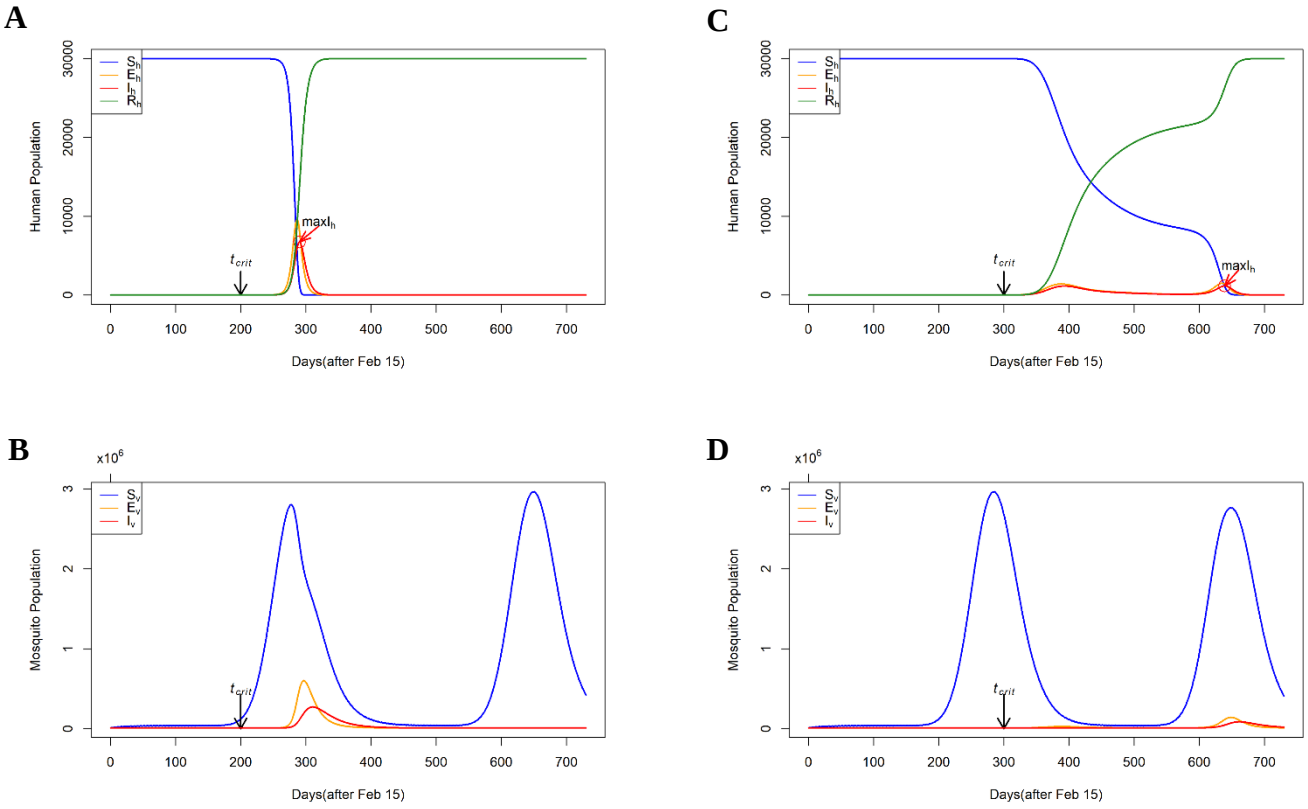


**Fig 2. The epidemic progression in the human and mosquito populations.** The y-axis is the number of humans or mosquitoes in the simulation and the x-axis is days after the simulation start date of February 15. $t_{crit}$ = arrival date of infectious human; $maxI_h$ = the epidemic peak size, the maximum human infected at any given point during the simulation. (A) indicates the disease progression in the human population, for an arrival date of an infectious human, 200 days after simulation start (i.e. September 3). (C) indicates disease progression for an arrival date of an infectious human, 300 days after simulation start (i.e. December 12). (B) and (D) show the disease progression in the mosquito population for the respective dates of arrival. (A) shows a classical rapid epidemic, with a unimodal response, with the peak occurring few weeks after virus introduction; while (C) shows a prolonged period of lower level transmission, resulting in a bimodal response. Default parameters from Table 2 were used for these simulations, except for dates of arrival of infectious human.

Fig 3 shows our QOIs, for all dates over a calendar year (simulation start date of February 15). The timing and size of the epidemic peak vary inversely as a function of date of arrival, with shorter epidemic peak timing, producing higher peak incidence and vice versa. Epidemic peak time monotonically decreases as a function of the date of arrival until October (mid- autumn season), then reverses to an increase, with a steep spike in mid-December and reverts to a decrease (Fig 3). Similarly, epidemic peak size monotonically increases until October, then reverses to a steady decline until mid-December and reverts to an increase (Fig 3).

In part, these discontinuities are reflections of scoring each run for a single peak; and corresponds to the model behavior shifts from the classical rapid unimodal epidemic, to the bimodal and prolonged epidemics.

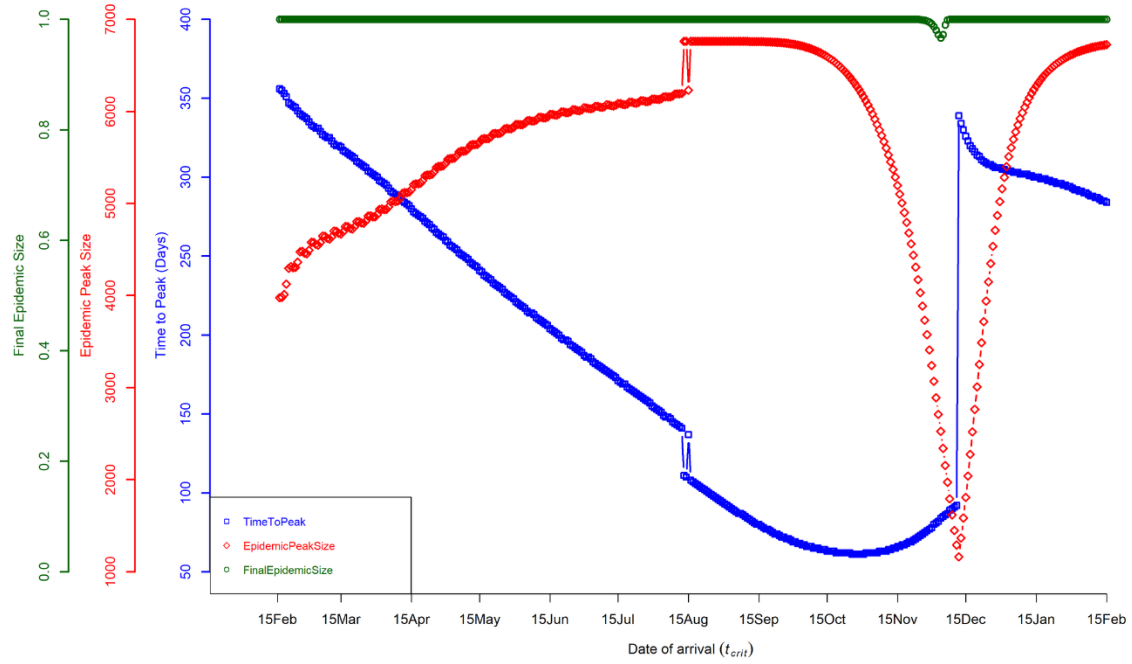


**Fig 3. Quantities of interest as a function of arrival date**. QOI vs date of arrival by calendar date. The x-axis is the date of arrival of an infectious human, simulation start date of February 15. The blue square points represent the time to peak infection in humans (in days). The red diamond points represent the maximum number of humans infected at any given point during the simulation. The green circle points represent the final (or cumulative) epidemic size at the end of the simulation; this is represented as the proportion of humans infected (rather than number). Simulations for arrivals on the 12 to 19 December, resulted in a prolonged low-level transmission, with bimodal peak, while other dates had a classical unimodal peak.
Note: We examined the fluctuation in the epidemic peak time and size on August 15, for a possible shift in model behavior, there was no change from the classical unimodal peak behavior observed around this date.

Overall, the shifts in epidemic dynamics are driven by the seasonal change (autumn and winter seasons) and its effect on transmission dynamics. Epidemic peak size was highest (with 23% of the susceptible population infected), for an arrival date on September 3rd, with a short time to peak of 90 days (Fig 2A). Epidemic peak size was lowest (with 0.04% of the susceptible population infected) for an arrival date on December 12th, with a longer time to peak of 339 days

(Fig 2C). All simulations ultimately infected 100% of the human population, except for arrival dates in mid-December, with a final epidemic size of 97% of the population (Fig 3).

These results show that under the conditions used here, an epidemic potential exists in all seasons of the year, with most favorable seasons for a large outbreak being in late summer/early autumn season. Epidemics occurring within this favorable period had an average epidemic peak size of 22% of the susceptible population infected, with a time to peak of 82 days. Arrival dates of an infectious human, in mid-autumn and early-winter season, can dramatically affect the epidemic dynamics.

**Seasonal variance and epidemic dynamics**

To examine the epidemic dynamics as a function of the seasonal temperature variance, we simulated two different sets of temperature regimes, with a fixed arrival date in mid-summer (August 15). In the first set of temperature regimes (historical; $T_{mean}$ varied from 19.0°C to 22.0°C and $T_{range}$ varied from 4.0°C to 6.0°C, both in increments of 0.2°C), the timing and magnitude of the epidemic peak vary inversely as a function of starting temperature (calculated for August 15 from $T_{mean}$ and $T_{range}$ using equation 16). Epidemic peak size increases monotonically with an increase in starting temperature, i.e. warmer temperatures at onset produce large epidemic peak size with a short peak time and vice versa (Fig 4A). The final epidemic size was insensitive to starting temperatures, as all simulations within this regime produced final epidemic sizes of 100% of the population infected.

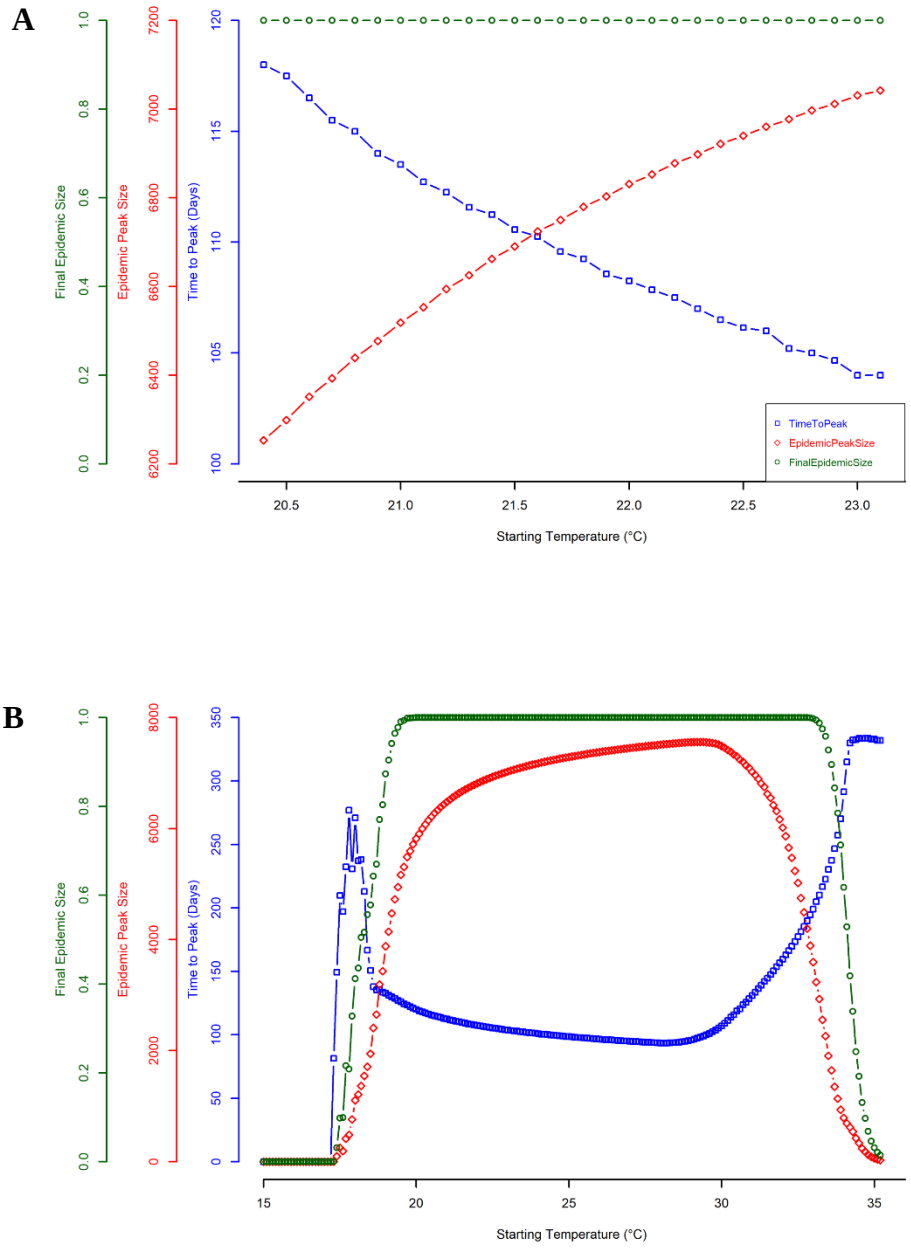


**Fig 4. Quantities of interest as a function of starting temperature**. The x-axis is the starting temperatures within each set of temperature regimes and the y-axis is the associated value of the QOIs being considered. Starting temperature is the temperature on August 15 calculated from $T_{mean}$ and $T_{range}$. The blue square points represent the time to peak infection in humans (in days). The red diamond points represent the maximum number of humans infected at any given point during the simulation. The green circle points represent represents the final (or cumulative) epidemic size at the end of the simulation; this is represented as the proportion of humans infected (rather than number). (A) represents the historical temperature regimes, given by $T_{mean}$ varied from 19°C to 22°C and $T_{range}$ varied from 4°C to 6°C (both in increments of 0.2°C), a total of 121 simulations. (B) represents the second set of temperature regimes, given by $T_{mean}$ varied from 15°C to 30°C and $T_{range}$ varied from 0°C to 15.0°C, total of 5776 simulations. Due to the fixed starting date, multiple combinations of $T_{mean}$ and $T_{range}$ had the same starting temperature. As no other parameters were varied in these simulation sets, QOI and model behavior was

identical for simulations with the same starting temperatures and overlapping points are not visible on the graphs. The default parameters from Table 2 were used for these simulations.

In the second set of temperature regimes (future; $T_{mean}$ varied from 15.0°C to 30.0°C and $T_{range}$ varied from 0.0°C to 15.0°C, both in increments of 0.2°C), epidemic peak time and size show similar inverse variation as a function of starting temperature, although the overall behavior is different. Epidemic peak size had a unimodal distribution with its peak at ~30 ºC and declines rapidly afterwards (conversely the time to peak decreases until 30 ºC). At this peak of ~30 ºC, the epidemic peak size was at 26% of the susceptible population infected, within a short peak time of 55 days. On the other hand, the final epidemic size steeply increases as a function of starting temperature, and plateaus at 20 ºC to 34 ºC (with 100% of the population infected), before steeply declining (Fig 4B). No epidemic occurred at lower starting temperatures of 15-17 ºC.

To further examine how mean temperature and seasonal variance combined to influence the epidemic size, Fig 5 shows the variation in the final epidemic size across the annual temperature bands. Thermal environments of mean annual temperatures between ~18 ºC to 28 ºC support high epidemic size, at both low and high seasonal variance. Mean annual temperature bands between ~28 ºC to 30 ºC supports a high epidemic size at low seasonal variance, this steadily diminishes as seasonal variance increases. No epidemic was produced at low mean annual temperatures of 15 ºC to ~17 ºC and corresponding low seasonal variance. In general, under the conditions used here, the dynamics of the epidemic are largely driven by the seasonal variation in temperature.

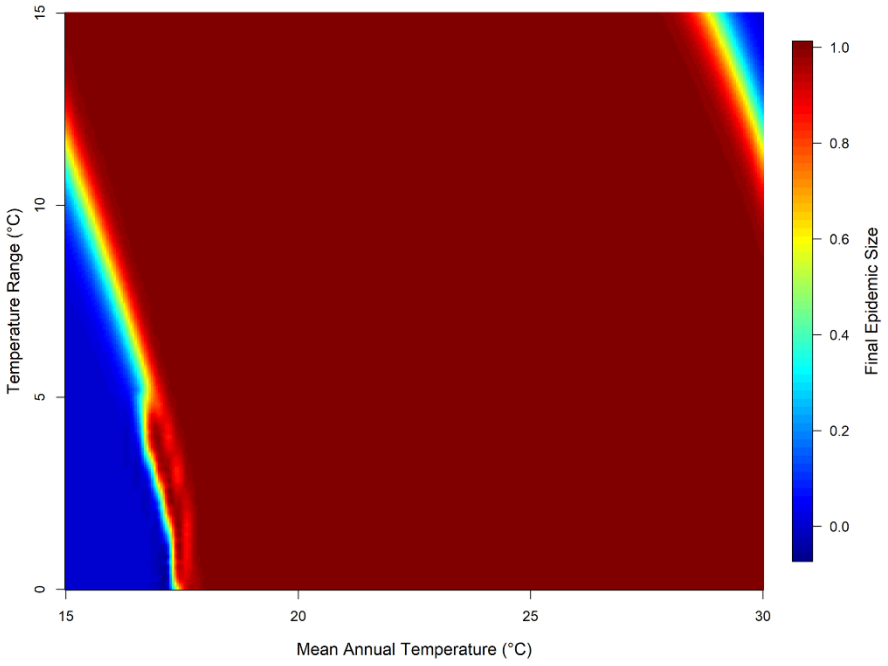


**Fig 5. Final epidemic size across different seasonal temperature regimes.** Heat map of final epidemic size (represented as the proportion of humans infected rather than number) as a function of mean annual temperature and temperature range. Temperature regimes here is given by $T_{mean}$ varied from 15°C to 30°C and $T_{range}$ varied from 0°C to 15°C, a total of 5776 simulations. Default parameters from Table 2 were used for these simulations, except for temperature parameters.

## Model sensitivity analysis

Model sensitivity was characterized using 500 simulations runs for dengue parameter ranges as given in Table 2. All parameters were uniformly distributed for the LHS sampling. The conditions here were also permissive for epidemics, with ($I_h > 2$) in 498 of the 500 simulated parameter sets. The epidemic progression in these parameter sets was consistent with the general model behavior seen in Figs 2A and 2C (i.e. a combination of unimodal and bimodal responses). The distribution of the QOIs had a wider range of values ( i.e. $MaxI_h$ =18 to 9537 humans infected; $tmaxI_h$ = 20 to 689 days from $t_{crit}$; $cumI_h$ = 72% to 100% of the population infected), thus providing more variation in the sensitivity analysis.

Table 3 shows the relative importance of the input parameters to our QOIs, using uniform LHS distributions for dengue parameters (Table 2). Considering the main effects only, under the parameter variation used, epidemic peak characteristics were sensitive to the arrival date of the infectious human and mean annual temperature. The final epidemic size was more sensitive to the mosquito life history trait parameters. Other influential parameters on all the QOIs were the mosquito biting rate, transmission rates, and mosquito recruitment. Our QOIs were least sensitive to the temperature range parameter (Table 3).

**Table 3. Sensitivity analysis of the model's QOIs.**

| Parameter | $MaxI_h$ | $tmaxI_h$ | $cumI_h$ |
|---|---|---|---|
| $t_{crit}$ | 1.00 (-0.36) | 1.00 (-0.17) | 0.29 (0.01) |
| $T_{mean}$ | 1.00 (-0.19) | 1.00 (0.12) | 0.46 (0.03) |
| $T_{range}$ | 0.27 (0.00) | 0.27 (0.00) | 0.32 (-0.01) |
| $a$ | 0.97 (-0.10) | 1.00 (0.22) | 1.00 (-0.12) |
| $\beta_{h\to v}$ | 0.63 (0.04) | 1.00 (-0.25) | 1.00 (0.11) |
| $\beta_{v\to h}$ | 1.00 (0.19) | 1.00 (-0.23) | 0.98 (0.10) |
| $\mu_v$ | 0.52 (-0.03) | 1.00 (0.20) | 0.90 (-0.08) |
| $\gamma_v$ | 0.92 (0.09) | 0.89 (-0.06) | 0.44 (0.03) |
| $iv$ | 0.27 (0.00) | 0.49 (0.02) | 0.29 (0.01) |
| $q$ | 0.34 (-0.01) | 0.53 (0.02) | 0.17 (0.00) |
| $R_{tot}$ | 1.00 (0.14) | 1.00 (-0.12) | 0.97 (0.10) |

Relative importance and model averaged parameter coefficient from best-supported models (confidence set of models, see appendix for details). The relative importance of parameters on a scale between 0.00 and 1.00; the model-averaged coefficients for parameters in parentheses - effects are summarized by their direction $(+|-)$, positive indicates the QOI increases as the parameter increases, while negative indicates QOI decreases as the parameter increases. Before model fitting, parameters were centered on zero and scaled to unit variance, to normalize parameters within the same range, hence coefficient estimates are within the range of 0.0 to 1.0. QOI is denoted by: $maxI_h$ = the epidemic peak size; $tmaxI_h$ = time to peak; $cumI_h$ = final epidemic size. Notations and descriptions of parameters are denoted in Table 2.

Epidemic peak size was sensitive to the interaction term between the arrival date of an infectious human and temperature range, while neither epidemic peak time nor the final epidemic size was sensitive to this interaction term. None of the QOIs were sensitive to the interaction term of arrival date and mean annual temperature. Some other interactive terms that were

influential to all QOIs include interactions (terms) between arrival date of an infectious human and the mosquito life history trait parameters (i.e. biting rate, transmission rates, and recruitment). Interactions between transmission rates and other parameters had high relative importance for epidemic peak and final sizes, indicating that transmission rates may alter the effect of other parameters (See S8 Table for full details).

Epidemic peak size was sensitive to the interaction term between the arrival date of an infectious human and temperature range, while neither epidemic peak time nor the final epidemic size was sensitive to this interaction term. None of the QOIs were sensitive to the interaction term of arrival date and mean annual temperature. Some other interactive terms that were influential to all QOIs include interactions (terms) between arrival date of an infectious human and the mosquito life history trait parameters (i.e. biting rate, transmission rates, and recruitment). Interactions between transmission rates and other parameters had high relative importance for epidemic peak and final sizes, indicating that transmission rates may alter the effect of other parameters (See S8 Table for full details).

## Discussion

We extend the Lord et al. (unpublished work) model for chikungunya in *A. aegypti* and *A. albopictus* mosquitoes in Florida to a deterministic compartmental model for dengue fever in in *A. aegypti* in Madeira Island. This SEI-SEIR model explores dengue epidemic dynamics as triggered by the arrival of an infected person in Funchal, Madeira and the effects of seasonally varying temperature on transmission. Our analysis focused on three quantities of interest: time to epidemic peak, epidemic peak size and the final size of the epidemic. We then used a global sensitivity analysis to determine which input parameters were most important to quantities of interest.

With the simulations of our model, we show that the date of arrival of an infected human in a susceptible human population dramatically affects the timing and magnitude of an epidemic peak. Given the default parameter values used here, the arrival of an infected person at any time

within a calendar year in Funchal can evolve into an epidemic producing a sizable outbreak. Outbreaks starting with the arrival of the infected human at the beginning of winter (i.e. in December), took a longer time to peak, with a resulting bimodal outbreak response. These arrivals coincided with the depletion of the mosquito population; hence an initial small outbreak occurs, then a prolonged low-level transmission until the number of susceptible mosquitoes is replenished (at the next seasonal peak recruitment), then another outbreak occurs. This suggests the temporal dynamics of the mosquito population is important in determining the epidemic dynamics. This also suggests that the virus can remain viable within the population at low rates, until the next favorable season for transmission.

In contrast, arrival at the end of summer (late August), and early autumn (September and October) produces epidemics with a much faster peak rate and a corresponding large epidemic size. These transient epidemics are indicative of a higher transmission potential at this point of the year and are consistent with the scenario of the 2012 outbreak [6]. In this outbreak, the epidemic peaked approximately one month following the initial cases, with a resultant large epidemic size [7]. This also further reiterates the conclusions of [8], regarding the time point in the year with the highest epidemic risk and when local control strategies should be intensified. The overall model behavior in response to the timing of virus introduction within the susceptible population is similar to other previous dengue models [26, 60]

Furthermore, we showed the interaction between seasonal temperature mean and range in determining the timing and size of an epidemic peak. The historical decadal weather data for Funchal, Madeira had an annual mean temperature of 20ºC and an average seasonal temperature range of 5ºC, a highly suitable thermal environment for the vectorial capacity of *A. aegypti* mosquitoes and arbovirus transmission. As expected, all our model simulations for this set of temperature regimes evolved into an epidemic. Both epidemic peak size and time to peak responded monotonically to starting temperature, with warmer temperatures at onset producing high prevalence and faster peaks. Subsequently, when we widened the temperature regimes the epidemic peak size responded unimodally to starting temperature, with a peak at ~30ºC.

Extending the temperature regimes allowed us to demonstrate the nonlinear influence of the interaction between annual mean temperature and range on epidemic dynamics. At a low annual mean temperature (15ºC to 17ºC) and range (0ºC to ~10ºC), no epidemic occurred; however, this temperature band becomes suitable for transmission as the temperature range increases beyond this point. Intermediate annual mean temperatures (~18ºC to ~28ºC), supported epidemic transmission at both low and high temperature range (i.e. 0ºC to 15ºC). Epidemics introduced within these temperature regimes had the highest epidemic suitability (using final epidemic size as a measure of epidemic suitability). Lastly, at high annual mean temperatures (> 28ºC to 30ºC) and range (0ºC to ~10ºC), transmission was supported with high epidemic suitability. However, epidemic suitability diminishes as temperature range increases.

To reiterate, most of the simulated temperatures are very unlikely to occur in Funchal, with the exception of sporadic extreme summer temperatures and heat waves. Such sporadic extreme events have been documented, with recent abrupt changes in temperatures on the island [53, 54]. Hence our simulations give an estimate of epidemic suitability in the presence of these extreme temperature conditions. Overall these distinct thermal responses are similar to those discussed in the works of [17] and [18], which investigated the effects of temperature on dengue transmission. Other models (e.g. [13, 19, 61] have shown that the influence of temperature on other mosquito life history traits (e.g. biting rates and population size) can contribute significantly to transmission dynamics. Although we did not consider these factors, our results provide insights about suitable thermal environments for dengue transmission and potential epidemic suitability in Funchal, Madeira.

Our sensitivity analysis further characterizes the variability in epidemic dynamics as a function of the arrival date of one infectious human into the susceptible population and the seasonal temperature regime. There was a significant difference between the sensitivity of the quantities of interest to the parameters. The timing and magnitude of the epidemic peak were more sensitive to parameter variation in arrival date and mean annual temperature, than the final epidemic size. So, slight changes in the parameter values will have more effect on the epidemic peak characteristics. Overall the quantities of interest were sensitive to the biting rate,

transmission rates, and mosquito population size. This is consistent with other modeling studies that highlight the importance of the mosquito dynamics on epidemic outcomes [27, 62, 63].

Our sensitivity analysis went one step further by characterizing the interaction effects between the parameters on the epidemic dynamics. Though this was not the focus of our analysis, it can be useful for improving understanding of the complex processes that interact to determine epidemic dynamics. Likewise, from a control and mitigation perspective, the interaction term effects are useful to understand how the implementation of a specific control strategy can have dramatic effects on the mosquito life history traits and in turn the overall epidemic dynamics. A cautionary note, our sensitivity analysis varied only the mosquito portion of the transmission cycle and does not account for the variance in the human transmission and its combined influence on the epidemic dynamics.

Putting this all together, our model could be used as a mathematical tool to study different epidemic scenarios and shifts in epidemic suitability for other regions in Madeira Island. Near term projection for seasonal temperature variation for the region of Madeira island (i.e. the North Atlantic, Europe and Mediterranean region), predicts a warming of ~2°C in annual mean temperature, with summer months of June, July and August (JJA) temperatures warming up to ~2.9°C [52, 64]. Considering the implications of this in view of our results, we can speculate that the south coast region of Madeira Island (where Funchal is located), would continue to support potential year-round transmission, with possible higher epidemic suitability. The north coast and inland regions of the island, where current climate suggests limited or no epidemic suitability could have an increased potential to support transmission in extreme summer months. It is important to note that these projected shifts in epidemic suitability will also be influenced by other factors like rainfall, humidity, and anthropogenic activities. Thus, seasonal temperature variation must be considered jointly with these factors.

It is worth reiterating that the default parameters values used in our model were permissive for epidemics and likely more permissive than the real world. Likewise, our model made several assumptions for convenience and does not cover the full complexities of mechanistic drivers of an epidemic. We did not consider rainfall, which would play an important

role in the mosquito seasonality and life traits in relationship to climate change. We also did not consider the scenario of multiple serotypes of dengue co-circulating in the population, and thus prior exposure can lead to immune interactions (a possibility for Funchal, given the circulating serotype for the 2012 outbreak was DENV I). We also assumed a non-dynamic human population, however, human movement could play an important role in patterns of transmission and introduction (given the constant influx of tourists all year round on the island). We also did not consider vector surveillance and control measures implemented on the island, which is an important factor in limiting mosquito density.

In summary, the model presented here is relevant for the introduction of a new dengue serotype into Funchal, Madeira Island and the interaction between mean temperature and seasonal variation to drive the epidemic dynamics. Our results demonstrate the potential for all year transmission of dengue, with varying levels of epidemic suitability, following an introduction of the virus. Overall, we demonstrated that epidemic dynamics are strongly influenced by variation in the date of arrival, seasonal temperature, biting rate, transmission rates, and the mosquito population. The model sensitivity analysis provides insight into the relative importance of these parameters and their interactive effects as mechanistic drivers of an epidemic. These results can be a useful guide in the development of effective local control and mitigation strategies for dengue fever in Madeira Island.

## References

1. Messina JP, Brady OJ, Golding N, Kraemer MUG, Wint GRW, Ray SE, et al. The current and future global distribution and population at risk of dengue. Nat Microbiol. 2019. doi: https://doi.org/10.1038/s41564-019-0476-8.

2. Kraemer MUG, Hay SI, Pigott DM, Smith DL, Wint GRW, Golding N. Progress and challenges in infectious disease cartography. Trends Parasitol. 2016;32(1):19-29. doi: https://doi.org/10.1016/j.pt.2015.09.006.

3. Leta S, Beyene TJ, De Clercq EM, Amenu K, Kraemer MUG, Revie CW. Global risk mapping for major diseases transmitted by *Aedes aegypti and Aedes albopictus*. Int J Infect Dis. 2018;67:25-35. doi: https://doi.org/10.1016/j.ijid.2017.11.026.

4. Margarita Y, Grácio AS, Lencastre I, Silva A, Novo T, Sousa C. First record of *Aedes (stegomyia) aegypti* (Linnaeus, 1762) (Diptera, culicidae) in Madeira Island - Portugal (in portguese) Acta Parasitol Port.. 2006;13:59-61.

5. Medlock JM, Hansford KM, Schaffner F, Versteirt V, Hendrickx G, Zeller H, et al. A review of the invasive mosquitoes in europe: ecology, public health risks, and control options. Vector Borne Zoonotic Dis. 2012;12(6):435-47. doi: https://doi.org/10.1089/vbz.2011.0814.

6. ECDC. Dengue outbreak in madeira (2012-13) 2013. European Centre for Disease Prevention and Control [17 Jul 2019]. Available from: https://ecdc.europa.eu/en/dengue-fever/threats-and-outbreaks/madeira-outbreak-2012.

7. ECDC. Update on autochthonous dengue cases in Madeira, Portugal. Stockholm: European Centre for Disease Prevention and Control, 2012. Available from: https://ecdc.europa.eu/sites/portal/files/media/en/publications/Publications/dengue-madeira-risk-assessment-update.pdf.

8. Lourenco J, Recker M. The 2012 Madeira dengue outbreak: epidemiological determinants and future epidemic potential. PLoS Negl Trop Dis. 2014;8(8):e3083. doi: https://doi.org/10.1371/journal.pntd.0003083.

9. Watts DM, Burke DS, Harrison BA, Whitmire RE, Nisalak A. Effect of temperature on the vector efficiency of *Aedes aegypti* for dengue 2 virus. Am J Trop Med Hyg.1987;36(1):143-52. doi: https://doi.org/10.4269/ajtmh.1987.36.143.

10. Rueda LM, Patel KJ, Axtell RC, Stinner RE. Temperature-dependent development and survival rates of *Culex quinquefasciatus* and *Aedes aegypti* (Diptera: Culicidae). J Med Entomol. 1990;27(5):892-8. doi: https://doi.org/10.1093/jmedent/27.5.892

11. Eisen L, Monaghan AJ, Lozano-Fuentes S, Steinhoff DF, Hayden MH, Bieringer PE. The impact of temperature on the bionomics of *Aedes (stegomyia) aegypti*, with special reference to

the cool geographic range margins. J Med Entomol. 2014;51(3):496-516. doi: https://doi.org/10.1603/ME13214

12. Couret J, Dotson E, Benedict MQ. Temperature, larval diet, and density effects on development rate and survival of *Aedes aegypti* (Diptera: Culicidae). PloS One. 2014;9(2):e87468. doi: https://doi.org/10.1371/journal.pone.0087468.

13. Yang HM, Macoris ML, Galvani KC, Andrighetti MT, Wanderley DM. Assessing the effects of temperature on the population of *Aedes aegypti*, the vector of dengue. Epidemiol Infect. 2009;137(8):1188-202. doi: https://doi.org/10.1017/s0950268809002040.

14. Johansson MA, Powers AM, Pesik N, Cohen NJ, Staples JE. Nowcasting the spread of chikungunya virus in the Americas. PloS One. 2014;9(8):e104915. doi: https://doi.org/10.1371/journal.pone.0104915.

15. Liu-Helmersson J, Stenlund H, Wilder-Smith A, Rocklöv J. Vectorial capacity of *Aedes aegypti*: effects of temperature and implications for global dengue epidemic potential. PloS One. 2014;9(3):e89783. doi: https://doi.org/10.1371/journal.pone.0089783.

16. Morin CW, Monaghan AJ, Hayden MH, Barrera R, Ernst K. Meteorologically driven simulations of dengue epidemics in San Juan, PR. PLoS Negl Trop Dis. 2015;9(8):e0004002. doi: https://doi.org/10.1371/journal.pntd.0004002.

17. Mordecai EA, Cohen JM, Evans MV, Gudapati P, Johnson LR, Lippi CA, et al. Detecting the impact of temperature on transmission of zika, dengue, and chikungunya using mechanistic models. PLoS Negl Trop Dis. 2017;11(4):e0005568. doi: https://doi.org/10.1371/journal.pntd.0005568.

18. Huber JH, Childs ML, Caldwell JM, Mordecai EA. Seasonal temperature variation influences climate suitability for dengue, chikungunya, and zika transmission. PLoS Negl Trop Dis. 2018;12(5):e0006451. doi: https://doi.org/10.1371/journal.pntd.0006451.

19. Mordecai EA, Caldwell JM, Grossman MK, Lippi CA, Johnson LR, Neira M, et al. Thermal biology of mosquito-borne disease. Ecol Lett. 2019;0(0). doi: https://doi.org/10.1111/ele.13335.

20. Fernandopullé D. Climatic characteristics of the Canary Islands. In: G. K, editor. Biogeography and ecology in the Canary Islands: Springer, Dordrecht; 1976. p. 185-206.

21. Santos FD, Valente MA, Miranda PMA, Aguiar A, Azevedo EB, Tomé AR, et al. Climate change scenarios in the Azores and Madeira Islands. World Resour Rev. 2004;16(4):473-91. http://idlcc.fc.ul.pt/pdf/SantosEtalWRR2004.pdf.

22. Seixas G, Jupille H, Yen P-S, Viveiros B, Failloux A-B, Sousa CA. Potential of *Aedes aegypti* populations in Madeira Island to transmit dengue and chikungunya viruses. Parasit Vectors. 2018;11(1):509. doi: https://doi.org/10.1186/s13071-018-3081-4.

23. Messina JP, Brady OJ, Pigott DM, Brownstein JS, Hoen AG, Hay SI. A global compendium of human dengue virus occurrence. Sci Data. 2014;1:140004. doi: https://doi.org/10.1038/sdata.2014.4.

24. Guo C, Zhou Z, Wen Z, Liu Y, Zeng C, Xiao D, et al. Global epidemiology of dengue outbreaks in 1990-2015: A systematic review and meta-analysis. Front Cell Infect Microbiol. 2017;7:317-. doi: https://doi.org/10.3389/fcimb.2017.00317.

25. Ryan SJ, Carlson CJ, Mordecai EA, Johnson LR. Global expansion and redistribution of aedes-borne virus transmission risk with climate change. PLoS Negl Trop Dis. 2019;13(3):e0007213. doi: https://doi.org/10.1371/journal.pntd.0007213.

26. Otero M, Solari HG. Stochastic eco-epidemiological model of dengue disease transmission by *Aedes aegypti* mosquito. Math Biosci. 2010;223(1):32-46. doi: https://doi.org/10.1016/j.mbs.2009.10.005.

27. Manore CA, Hickmann KS, Xu S, Wearing HJ, Hyman JM. Comparing dengue and chikungunya emergence and endemic transmission in *A. aegypti* and *A. albopictus*. J Theor Biol. 2014;356:174-91. doi: https://doi.org/10.1016/j.jtbi.2014.04.033.

28. Karl S, Halder N, Kelso JK, Ritchie SA, Milne GJ. A spatial simulation model for dengue virus infection in urban areas. BMC Infect Dis. 2014;14:447. doi: https://doi.org/10.1186/1471-2334-14-447.

29. Ferreira CP, Godoy WAC. Ecological modelling applied to entomology. Switzerland: Springer; 2014.

30. Institute of Health Administration, IP-RAM. Mosquito on Madeira Island (in portguese). Institute of Health Administration, IP-RAM, Regional Secretariat of Health, Autonomous Region of Madeira; 2019 [17 Jul 2019]. Available from: http://doc.iasaude.pt/mosquito/index.php/mosquito/mosquito-na-ilha-da-madeira.

31. Newton EA, Reiter P. A model of the transmission of dengue fever with an evaluation of the impact of ultra-low volume (ulv) insecticide applications on dengue epidemics. The Am J Trop Med Hyg. 1992;47(6):709-20. doi: https://doi.org/10.4269/ajtmh.1992.47.709.

32. Menach AL, McKenzie FE, Flahault A, Smith DL. The unexpected importance of mosquito oviposition behaviour for malaria: non-productive larval habitats can be sources for malaria transmission. Malar J. 2005;4(1):23. doi: https://doi.org/10.1186/1475-2875-4-23.

33. Institute of Health Administration, IP-RAM. Entomological panel bulletins(in portguese). IASAÚDE IP-RAM, Sanitary Engineering Unit: Institute of Health Administration, IP-RAM, Regional Secretariat of Health, Autonomous Region of Madeira, 2019. Available from: http://doc.iasaude.pt/mosquito/index.php/boletins/entomologicos.

34. Trpis M, Hausermann W. Dispersal and other population parameters of *Aedes aegypti* in an African village and their possible significance in epidemiology of vector-borne diseases. Am J Trop Med Hyg. 1986;35(6):1263 - 79. doi: https://doi.org/10.4269/ajtmh.1986.35.1263.

35. Lourenco J, Recker M. Dengue serotype immune-interactions and their consequences for vaccine impact predictions. Epidemics. 2016;16:40-8. doi: https://doi.org/10.1016/j.epidem.2016.05.003.

36. Paupy C, Ollomo B Fau - Kamgang B, Kamgang B Fau - Moutailler S, Moutailler S Fau - Rousset D, Rousset D Fau - Demanou M, Demanou M Fau - Herve J-P, et al. Comparative role of *Aedes albopictus* and *Aedes aegypti* in the emergence of dengue and chikungunya in central Africa. Vector Borne Zoonotic Dis. 2010;10(3). doi: https://doi.org/10.1089/vbz.2009.0005.

37. Lord CC. The effect of multiple vectors on arbovirus transmission. Isr J Ecol Evol. 2010;56(3-4):371-92. doi: https://doi.org/10.1560/ijee.55.3-4.371.

38. Focks DA, Barrera R. Dengue transmission dynamics: Assessment and implications for control. CiteSeer: World health organization on behalf of the special programme for research and training in tropical diseases, 2007. Available from: http://citeseerx.ist.psu.edu/viewdoc/summary?doi=10.1.1.612.689.

39. Nishiura H, Halstead SB. Natural history of dengue virus (DENV)-1 and DENV-4 infections: reanalysis of classic studies. J Infect Dis. 2007;195(7):1007–13. doi: https://doi.org/10.1086/511825.

40. Chan M, Johansson MA. The incubation periods of dengue viruses. PloS One. 2012;7(11):e50972. doi: https://doi.org/10.1371/journal.pone.0050972.

41. Gubler DJ, Suharyono W, Tan R, Abidin M, Sie A. Viraemia in patients with naturally acquired dengue infection. Bull World Health Organ. 1981;59(4):623-30. https://www.ncbi.nlm.nih.gov/pubmed/6976230

42. Vaughn DW, Green S, Kalayanarooj S, Innis BL, Nimmannitya S, Suntayakorn S, et al. Dengue viremia titer, antibody response pattern, and virus serotype correlate with disease severity. J Infect Dis. 2000;181(1):2-9. doi: https://doi.org/10.1086/315215

43. Santo António Parish Council. History of Santo António parish council (in portguese): junta de freguesia de Santo António- an autonomous region of Madeira; 2018 [17 Jul 2019]. Available from: http://www.jf-santoantonio.pt/historia.

44. Weather Underground. Weather history for Funchal Madeira (2008-2018) 2019 [01 Mar 2019]. Available from: https://www.wunderground.com/history/daily/pt/funchal/LPMA.

45. Funchal city hall. Funchal natural history museum: Funchal city hall (Câmara municipal do Funchal) 2019. Available from: http://www.cm-funchal.pt/pt/servi%C3%A7os/ci%C3%AAncia/museu-de-hist%C3%B3ria-natural-do-funchal/sobre-o-museu.html.

46. Andraud M, Hens N, Marais C, Beutels P. Dynamic epidemiological models for dengue transmission: a systematic review of structural approaches. PloS One. 2012;7(11):e49085. doi: https://doi.org/10.1371/journal.pone.0049085.

47. Kiraly A, Janosi IM. Stochastic modeling of daily temperature fluctuations. Phys Rev. 2002;65(1539-3755 (Print)):051102 1-6. doi: https://doi.org/10.1103/PhysRevE.65.051102.

48. Lord CC, Day JF. Simulation studies of st. louis encephalitis virus in south Florida. Vector Borne Zoonotic Dis. 2001;1(4):299-315. doi: https://doi.org/10.1089/15303660160025921.

49. Lord CC, Day JF. Simulation studies of st. louis encephalitis and west nile viruses: the impact of bird mortality. Vector Borne Zoonotic Dis. 2001;1(4):317-29. doi: https://doi.org/10.1089/15303660160025930.

50. MathWorks. MATLAB and Statistics Toolbox Release 2016a. Natick, Massachusetts: The MathWorks Inc.; 2016.

51. R-Core-Team. The R project for statistical computing: CRAN; 2019. Available from: https://www.r-project.org/.

52. IPCC. Climate change 2013: The physical science basis. Contribution of working group i to the fifth assessment report of the intergovernmental panel on climate change. Cambridge University Press, Cambridge, United Kingdom, and New York, NY, USA: 2013; [1535]. Available from: https://www.ipcc.ch/report/ar5/wg1/.

53. Madeira Island News. Madeira heatwave continues. Madeira Island news, 2016 [17 Jul 2019]. Available from: https://www.madeiraislandnews.com/2016/08/heatwave-continues.html.

54. Madeira Island News. Hottest december day for 150 years. Madeira Island news, 2018 [17 Jul 2019]. Available from: https://www.madeiraislandnews.com/2018/12/hottest-december-day-for-150-years.html.

55. Marino S, Hogue IB, Ray CJ, Kirschner DE. A methodology for performing global uncertainty and sensitivity analysis in systems biology. J Theor Biol. 2008;254(1):178-96. doi: https://doi.org/10.1016/j.jtbi.2008.04.011.

56. Wu J, Dhingra R, Gambhir M, Remais Justin V. Sensitivity analysis of infectious disease models: methods, advances, and their application. J R Soc Interface. 2013;10(86):20121018. doi: https://doi.org/10.1098/rsif.2012.1018.

57. Hamby DM. A review of techniques for parameter sensitivity analysis of environmental models. Environ Monit Assess. 1994;32(2):135-54. doi: https://doi.org/10.1007/bf00547132.

58. Burnham KP, Anderson DR. Model selection and multimodel inference: a practical information-theoretic approach: Springer, New York, NY; 2002.

59. Calcagno V, de Mazancourt C. Glmulti: an R package for easy automated model selection with (generalized) linear models. 2010. 2010;34(12): J Stat Softw. doi: https://doi.org/10.18637/jss.v034.i12.

60. Erickson RA, Presley SM, Allen LJS, Long KR, Cox SB. A dengue model with a dynamic *Aedes albopictus* vector population. Ecol Model. 2010;221(24):2899-908. doi: https://doi.org/10.1016/j.ecolmodel.2010.08.036.

61. Yang HM, Macoris ML, Galvani KC, Andrighetti MT, Wanderley DM. Assessing the effects of temperature on dengue transmission. Epidemiol Infect. 2009;137(8):1179-87. doi: https://doi.org/10.1017/s0950268809002052.

62. Ellis AM, Garcia AJ, Focks DA, Morrison AC, Scott TW. Parameterization and sensitivity analysis of a complex simulation model for mosquito population dynamics, dengue transmission, and their control. Am J Trop Med Hyg. 2011;85(2):257-64. doi: https://doi.org/10.4269/ajtmh.2011.10-0516.

63. Ndii MZ, Hickson RI, Allingham D, Mercer GN. Modelling the transmission dynamics of dengue in the presence of *Wolbachia*. Math Biosci. 2015;262:157-66. doi: https://doi.org/10.1016/j.mbs.2014.12.011.

64. Seneviratne SI, Field CB, Barros V, Stocker TF, Dahe Q, Dokken DJ, et al. Managing the risks of extreme events and disasters to advance climate change adaptation. Cambridge: Intergovernmental panel on climate change 2012; [582]. Available from: https://www.ipcc.ch/report/managing-the-risks-of-extreme-events-and-disasters-to-advance-climate-change-adaptation/.